Acoustic Simulation of a Special Switched Reluctance Drive by Means of Field–Circuit Coupling and Multiphysics Simulation

M. van der Giet, E. Lange, D. A. P. Corrêa, I. E. Chabu, S. I. Nabeta, and K. Hameyer, *Senior Member, IEEE*

***Abstract*—The approach presented in this paper consists of an energy-based field–circuit coupling in combination with multiphysics simulation of the acoustic radiation of electrical machines. The proposed method is applied to a special switched reluctance motor with asymmetric pole geometry to improve the start-up torque. The pole shape has been optimized, subject to low torque ripple, in a previous study. The proposed approach here is used to analyze the impact of the optimization on the overall acoustic behavior. The field–circuit coupling is based on a temporary lumped-parameter model of the magnetic part incorporated into a circuit simulation based on the modified nodal analysis. The harmonic force excitation is calculated by means of stress tensor computation, and it is transformed to a mechanical mesh by mapping techniques. The structural dynamic problem is solved in the frequency domain using a finite-element modal analysis and superposition. The radiation characteristic is obtained from boundary element acoustic simulation. Simulation results of both rotor types are compared, and measurements of the drive are presented.**

***Index Terms*—Acoustic noise of electrical machines, field–circuit coupling numerical simulation, finite-element method (FEM), switched reluctance motor (SRM).**

I. Introduction

THE SWITCHED reluctance motor (SRM) considered in this paper presents an asymmetric pole geometry in the rotor with the purpose of improving the starting unidirectional torque in any rotor position. Despite the advantages achieved by such a design, the SRM presents an intrinsic nonnegligible torque ripple and force-density excitations, which are very troublesome because they produce vibration and audible noise. In a previous work, the torque ripple has been minimized while avoiding the degradations of the starting and mean torques. That has been accomplished by a multiobjective optimization technique coupled to finite-element (FE) analysis [1].

Manuscript received February 15, 2009; revised June 27, 2009, December 22, 2009, and April 11, 2010; accepted April 16, 2010. Date of publication June 10, 2010; date of current version August 11, 2010.

M. van der Giet, E. Lange, and K. Hameyer are with the Institute of Electrical Machines, RWTH Aachen University, 52056 Aachen, Germany (e-mail: mvdg@iem.rwth-aachen.de).

D. A. P. Corrêa is with the Centro Tecnológico da Marinha em São Paulo, São Paulo 05508-900, Brazil.

I. E. Chabu and S. I. Nabeta are with the Electrical Machines and Drives Laboratory (GMAcq), Escola Politécnica da Universidade de São Paulo, São Paulo 05508-900, Brazil.

Color versions of one or more of the figures in this paper are available online at http://ieeexplore.ieee.org.

Digital Object Identifier 10.1109/TIE.2010.2051935

In this study, the focus is set on the acoustic behavior of this SRM. In order to fully analyze the SRM acoustic behavior, this paper proposes an integrated approach using a multiphysics simulation, including field-circuit coupling as well as structure dynamics and the simulation of the acoustic radiation. As oppose to [2], the field-circuit simulation is implemented in a flexible way, including the drive circuitry and the analog control. A quantitative analysis of both the initial design and the optimized design is performed on all levels of the generation of audible noise: Simulated currents, force excitation spectra, body sound, and airborne sound are compared. It is shown in which way such an approach can help to analyze the influence of the rotor shape on the audible noise radiated from such an SRM.

The accurate simulation of the parasitic effects is strongly coupled to the exciting current waveforms. The numeric field-circuit coupled simulation, although expensive in terms of computation time, provides more accurate results compared to analytical approaches, e.g., magnetic equivalent circuits [3] or 3-D Fourier series expansion of the air-gap field [4]. The different numeric field-circuit coupled approaches can be distinguished by their numeric type of coupling. Numerical strongly coupled approaches combine the differential equations of both the field domain and the circuit domain in a single equation system [5], while numerical weakly coupled approaches assemble the equations for each domain separately and solve them independently [6], [7]. Since the time constants of the field and circuit domains differ by orders of magnitude, i.e., the short-circuit time of the electrical machine ($\approx$ ms) versus the switching time of the semiconductors ($\ll \mu$s), the strongly coupled approach has the disadvantage of unnecessarily solving the unknowns of the field domain around the nonlinear switching points of the circuitry. For the number of unknowns of the field domain of the SRM exceeding the number of unknowns of the circuit domain by orders of magnitude too, a numerical weakly coupled approach is being applied.

Classical analytical approaches for noise analysis in electrical machines rely on the identification of space and time harmonics in the air-gap field that generate radial magnetic force waves [8], [9]. The vibration response of the mechanical structure and the radiation characteristic can also be estimated using simple analytical formulas [8], which is, for example, used for optimization purposes [10].

Numerical simulations, e.g., the FE method (FEM), are able to capture finer details in the model and allow an accurate

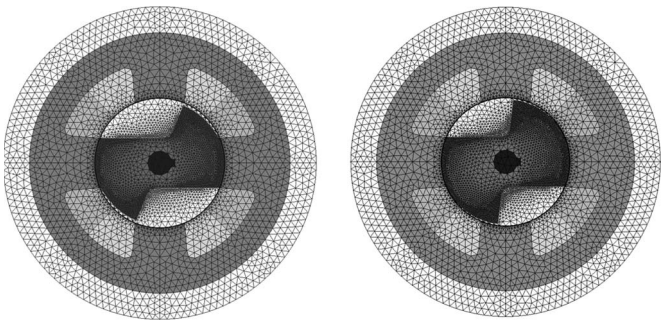

Fig. 1. Electromagnetic mesh: (left) reference design and (right) optimized design.

determination of air-gap field and magnetic force magnitudes, deformation, and radiation [9], [11], [12]. Under the standard linear assumption, the vibroacoustic problem is most commonly solved in the frequency domain either by modal analysis and superposition or by immediate harmonic analysis. The first method is applied in this paper. The radiation problem is approached using boundary element techniques.

This paper is outlined as follows: First, the SRM under analysis and the previous work on its optimization is reviewed briefly. Second, the combination of field–circuit coupling on the one hand and the multiphysics simulation (magnetic field, magnetic forces, mechanical deformation, and acoustic radiation) on the other hand is explained.

Afterward, numerical and experimental results are given and discussed. This paper is finalized by a summary and a conclusion.

II. Acoustic Analysis of SRM

A. Special SRM Design

In small-power drives, which are used in hand tools and light domestic appliances, traditional fractional horsepower motors are employed such as shaded-pole and universal types. These motors, in spite of their reliability and low cost, have several drawbacks, such as poor efficiency, low torque capability, and commutator and brush wear with high electromagnetic interference as in the universal type.

The SRM emerges as a solution that combines high reliability, good torque characteristics, high efficiency, and low cost [13]. In particular, for unidirectional drives, the proposed 4:2-pole two-phase SRM is the simplest electromagnetic structure available for such a motor. In order to ensure the starting torque at any rotor position, the rotor poles were designed with an asymmetrical geometry which provides a variable air gap as shown in Fig. 1 [14].

Nevertheless, the salient poles also produce torque ripple and cause vibration and acoustic noise. Thus, the challenge is to minimize such unwanted characteristics while keeping the starting and mean torques in the acceptable range. Many papers deal with this subject, e.g., [15] and [16].

B. Field–Circuit Approach

The field-circuit coupling is based on a temporary lumped-parameter model [17], seen from the terminals of the studied SRM, being incorporated into the circuit simulator, which is based on the modified nodal analysis. The nonlinear equation systems are solved by the Newton–Raphson method. If the state variable of the lumped-parameter model of the SRM is the current [18], the zeroth-order accurate expansion of the voltage drop of a single phase of the SRM is given by

$$\begin{aligned}\nu_{l,1}-\nu_{l,2} &= \partial_t \varphi\left(i(t),\Theta(t)\right)\\ &= L_{ls}^{\partial}\delta I_l + (\partial_\Theta \varphi_l)\delta\Theta. \end{aligned} \tag{1}$$

Herein, the first term represents the current-induced voltages, and the second term accounts for the motion-induced voltage. $\nu_{l,1}-\nu_{l,2}$ represents the terminal voltage of phase l, and L_{ls}^{∂} is the tangent inductance matrix. The phase currents are denoted I_l, the fluxes φ_l, and the rotation angle Θ; the linearized state variables are δI_l and $\delta\Theta$.

Whenever the energy of the SRM changes considerably, a new set of lumped parameters must be extracted from the FE model. This happens on a regular basis as the FE mesh needs to be modified, accounting for the rotation. The extraction is based on the balance of energy of the electrical machine, as presented in [19].

Let

$$M_{ij}(\mathbf{a})\, a_j = \int_\Omega \mathbf{j}\cdot\boldsymbol{\alpha}_i = \sum_l I_l W_{il} \tag{2}$$

be the nonlinear FE equations describing the SRM under phase currents. Herein, M_{ij} and a_j are the system matrix entries and the magnetic vector potentials of the discretized domain Ω, $\mathbf{j}$ is the current density, $\boldsymbol{\alpha}_i$ are the shape functions of the Galerkin scheme, and W_{il} can be regarded as the current shape functions of phase l.

Now, let I_l^* be the currents at time t and $b_i^* = I_l^* W_{il}$ the corresponding right-hand sides. Solving (2) with $b_I \equiv b_i^*$ and a fixed rotor angular position $\delta\Theta = 0$ gives a_j^*, and a first-order linearization around this particular solution writes

$$M_{ij}\left(a_j^*+\delta a_j\right) = M_{ij}\left(a_j^*\right)a_j^* + J_{ij}\left(a_j^*\right)\delta a_j = b_i^* + \delta b_i \tag{3}$$

with the Jacobian matrix $J_{ij} \equiv (\partial_{a_j} M_{ik}(a_j^*))a_k^*$. Since $M_{ij}(a_j^*)a_j^* = b_i^*$, one has

$$J_{ij}\left(a_j^*\right) \quad \delta a_j|_{\delta\Theta=0} = \delta b_i. \tag{4}$$

One can now repeatedly solve (4) with the right-hand sides $\delta b_i = \delta I_l W_{il}$ obtained by perturbating, one after the other, m phase currents I_l and obtain m solution vectors for $\delta a_j|_{\delta\Theta=0}$. Since (4) is linear, the magnitude of the perturbations δI_l is arbitrary. One can also define, by inspection, the tangent inductance matrix L_{ls}^{∂} of the SRM seen from the terminals as

$$\begin{aligned}\delta\varphi_l|_{\delta\Theta=0} &= W_{lj}\,\delta a_j|_{\delta\Theta=0}\\ &= W_{lj}J_{ji}^{-1}\left(a_j^*\right)W_{is}\,\delta I_s \equiv L_{ls}^{\partial}\,\delta I_s. \end{aligned} \tag{5}$$

One can now complement (5) to account for the motion-induced voltage (back electromotive force) for each phase l

$$\begin{aligned}E_l &= \partial_t\varphi_l = (\partial_\Theta\varphi_l)\dot\Theta\\ &= (\partial_\Theta\partial_{I_l}\Psi_M)\,\dot\Theta = (\partial_{I_l}\partial_\Theta\Psi_M)\,\dot\Theta = (\partial_{I_l}T)\,\dot\Theta \end{aligned} \tag{6}$$

where T is the torque and Ψ_M is the magnetic energy stored within the SRM. By recalling the energy conservation principals in (6), one avoids the tedious process of directly calculating the Θ derivative, i.e., slightly shift the rotor, solve the FE problem, evaluate new fluxes, and calculate a finite difference.

During the identification of the tangent inductance matrix described previously, it is thus easy to calculate additionally the torque corresponding to the perturbed solutions $\delta a_j|_{\delta\Theta=0}$ and to evaluate the motion-induced voltage E_l of each phase as the variation of torque with the perturbation of the corresponding phase current I_l. Beware however that, as the torque is a nonlinear function of the fields, the perturbations in this case need to be small. Because of the linearity of (4), one may scale the perturbation currents in (6) which yields

$$E_l = \frac{T\left(a_j^*\right) - T\left(a_j^* + \lambda\delta a_j|_{\delta\Theta=0}\right)}{\lambda\delta I_l}, \quad \text{with } \lambda = \kappa\frac{\left\|a_j^*\right\|_2}{\|\delta a_j\|_2}. \tag{7}$$

Herein, the scale factor is chosen between $0.01 \leq \kappa \leq 0.05$.

The presented approach to the field-circuit coupled problem is used to analyze the acoustic behavior of the special SRM. The 2-D FEM mesh of the SRM with original and optimized rotor shape is shown in Fig. 1. *Simplorer* is used as circuit simulator, and the circuit schematic is shown in Fig. 2. It can be seen that the complete supply circuit and the analog regulation part are modeled as part of the circuit. The hysteresis control, however, is implemented by means of *Simplorer* featured state machines (see bottom of Fig. 2).

C. Force Calculation

With the field distribution obtained from the coupled field–circuit simulation, the next step is to determine the electromagnetic force excitations.

Magnetic forces acting on a given medium are the divergence of the electromechanical tensor of that medium. Each medium has its own electromechanical tensor, and that of empty space, or air, is the celebrated Maxwell stress tensor [20]. In consequence, magnetic forces come under volume- and surface-density form. In saturable nonconducting materials, the volume density is basically related with the gradient of the magnetic reluctivity, and it is usually negligible with respect to the surface-force density $\Delta\sigma$. The latter one, located at material discontinuities (e.g., on the stator surface in the air gap), is the divergence in the sense of distribution of the electromechanical tensor. It can be shown [21] that it has a normal component only, whose amplitude is

$$\Delta\sigma_n = [b_n(h_{1n} - h_{2n}) - (w_1' - w_2')] \tag{8}$$

where b_n is the normal component of the magnetic flux density $\mathbf{b}$ at the interface between the stator and the air gap. h_{1n} and h_{2n} are the normal components of the magnetic field strength $\mathbf{h}$ in the air and in the stator iron, respectively. The magnetic coenergy density w' is related to the magnetic energy density w by

$$w' = \mathbf{h}(\mathbf{b}) \cdot \mathbf{b} - w(\mathbf{b}) = \mathbf{h}(\mathbf{b}) \cdot \mathbf{b} - \int_0^{|\mathbf{b}|} |\mathbf{h}(\mathbf{x})|\, d\mathbf{x}. \tag{9}$$

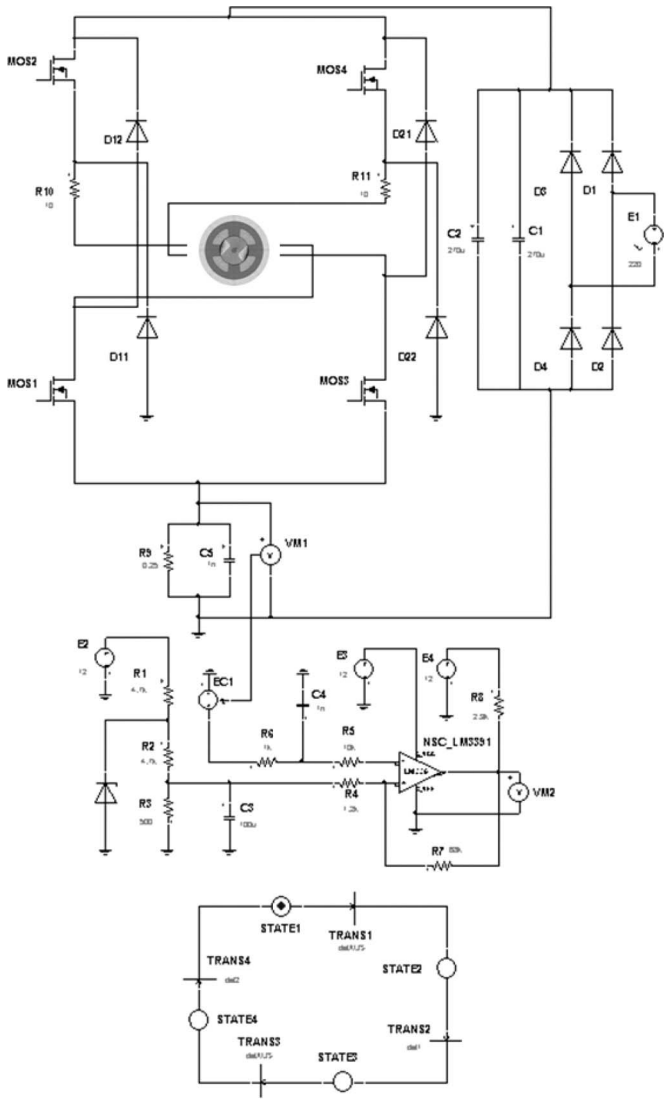

Fig. 2. Circuit model of the SRM with power electric circuit.

Due to the constant magnetic permeability of air, w_1' is

$$w_1' = \mathbf{h} \cdot \mathbf{b} - \frac{1}{2}\mathbf{h} \cdot \mathbf{b} = \frac{|\mathbf{b}|^2}{2\mu_0} \tag{10}$$

where μ_0 denotes the magnetic permeability of vacuum. As the magnetic steel sheets have a nonlinear magnetic characteristic, the magnetic force density is calculated by integrating the magnetic coenergy density w_2' in (8) along the magnetic flux density.

If the permeability of the iron can be considered to be constant, (8) can be simplified to

$$\Delta\sigma_n = \frac{1}{2}\left[b_n(h_{1n} - h_{2n}) - h_t(b_{1t} - b_{2t})\right]. \tag{11}$$

D. Vibroacoustic Analysis

1) Structure Dynamics: After the electromagnetic simulation of the SRM, a structure-dynamic simulation is performed to determine the vibration. The surface-force density on the

stator teeth, which is obtained from the electromagnetic simulation, is used as excitation.

The deformation-solver formulation is constructed using Hamilton's principle. After discretizing, the general vibration equation in the frequency domain is obtained

$$(\mathbf{K} + j\omega\mathbf{C} - \omega^2\mathbf{M}) \cdot \underline{\mathbf{d}}(\omega) = \underline{\mathbf{f}}(\omega) \tag{12}$$

where $\mathbf{K}$, $\mathbf{C}$, and $\mathbf{M}$ are the global stiffness and damping and mass matrix, respectively. The imaginary number is denoted by j, and ω describes the angular frequency of the problem. $\underline{\mathbf{d}}(\omega)$ is the vector of the complex nodal deformation, and $\underline{\mathbf{f}}(\omega)$ is the complex excitation force vector. As electrical machines typically can be considered low-damped systems [22], the term $j\omega\mathbf{C}$ is typically disregarded, as it is done in this work.

The complex surface-force density $\Delta\underline{\sigma}_n(\omega)$ is transformed from the electromagnetic simulation to a nodal force $\underline{\mathbf{f}}_k(\omega)$ on the mechanical model for each frequency to be analyzed. The force at node k is given by

$$\underline{\mathbf{f}}_k(\omega) = \sum_{j=1}^{n_e} \Delta\underline{\sigma}_{nj}(\omega) \int_{\Omega_m} \rho_j N_k \mathbf{e}_n \, d\Omega_m \tag{13}$$

where n_e is the number of elements of the electromagnetic mesh, $\Delta\underline{\sigma}_j(\omega)$ is the surface-force density on the jth element, $\mathbf{e}_n$ is the unit normal vector, Ω_m is the mechanical domain, and ρ_j and N_k are the element and nodal shape functions, respectively [23].

Then, the structure-dynamic simulation is performed. This can be done either by solving (12) directly for each individual frequency separately or by performing a modal analysis [24], i.e., finding the eigenvalues ω_i^2 and the corresponding eigenvectors $\mathbf{\Phi}_i$ in mass normalized form of the eigenproblem

$$\mathbf{K}\underline{\mathbf{d}}(\omega) = \omega^2\mathbf{M}\underline{\mathbf{d}}(\omega) \tag{14}$$

together with a subsequent modal superposition

$$\underline{\mathbf{d}}(\omega) = \sum_{i=1}^{N} \frac{\mathbf{\Phi}_i^T \underline{\mathbf{f}}(\omega)\mathbf{\Phi}_i}{\omega_i^2 - \omega^2} \tag{15}$$

where N is the number of eigenvalues. The latter approach is used in this work.

The mechanical model (Fig. 3) consists of all components of the electrical machine. The surrounding air is not included in the model, since for the expected small deformations of maximally a few micrometers, the influence of air on the deformation of the solid body is negligible. Thus, the coupling between structure-dynamic and acoustic simulations is considered as a unidirectional numerically weak coupling.

2) Acoustic Radiation: For the acoustic simulation, the mechanical deformation of the SRM is converted to the velocity ($\underline{v} = j\omega\underline{d}$). In principle, calculation of the acoustic fields is possible with the FEM. However, for calculation of airborne noise, this method is unfavorable, since the entire calculation area has to be discretized. An alternative is offered by the boundary element method (BEM). Here, only the surface of

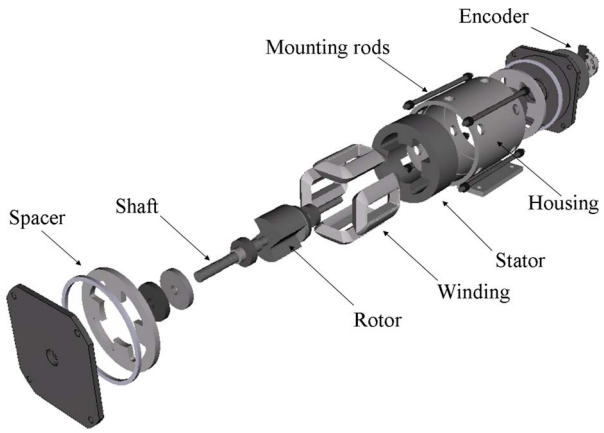

Fig. 3. Mechanical model of the SRM.

the SRM is discretized. The basic principle of the BEM is the solution of the Helmholtz differential equation

$$\Delta\underline{p} + k^2\underline{p} = 0 \tag{16}$$

with the complex sound pressure $\underline{p}$ and the wavenumber $k = \omega/c$ [25]. Here, c is the sound velocity of air. After further calculation, the following system results to

$$\underline{\mathbf{H}} \cdot \underline{\mathbf{p}} = \underline{\mathbf{G}} \cdot \underline{\mathbf{v}}. \tag{17}$$

$\underline{\mathbf{H}}$ and $\underline{\mathbf{G}}$ are the system matrices and the complex velocity vector. $\underline{\mathbf{v}}$ serves as the excitation value to the problem. A numerical solution of (17) results in the sound-pressure vector $\underline{\mathbf{p}}$. For the use of this method, an acoustic model of the radiating surface is needed. To decrease the numerical effort, the internal surface of the SRM is not included in the model. Therefore, the acoustic model consists of the simplified outer surface of the SRM's housing without holes. The mechanical velocity of the housing is transferred to this acoustic mesh [11].

Since the BEM is applied, sound-pressure and sound-particle velocities are evaluated on predetermined points or surfaces. As integral quantities, the acoustic power and the sound intensity of the SRM are calculated. The results are available at discrete frequencies.

III. Numerical and Experimental Results

A. Measurements

All tests are performed for rated conditions, i.e., 200 V dc, 1.7 A, and 6000 r/min. Fig. 4 shows the current and voltage waveforms as well as the rotation-related optical sensor signal for the optimized rotor. The vibration has been acquired by a piezoelectric accelerometer placed on the stator surface only in the tangential direction and coupled to a spectrum analyzer. As the aim of the initial study was the optimization regarding reluctance torque, the radial acceleration was not measured on the test bench. Therefore, the complete vibration behavior can only be described by means of numerical simulations.

The power efficiency was measured for both machines. Using the reference rotor, an efficiency of 69.0% was obtained, where the optimized rotor yielded 69.3%. For the calculation of the

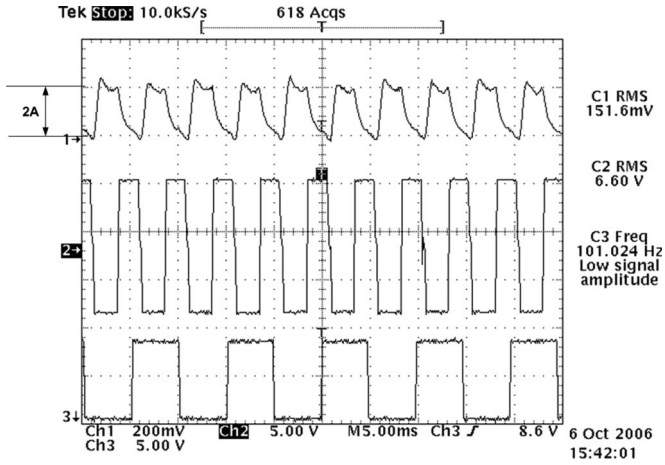

Fig. 4. Measurements with optimized rotor. (From top) Current, voltage, and optical sensor signal.

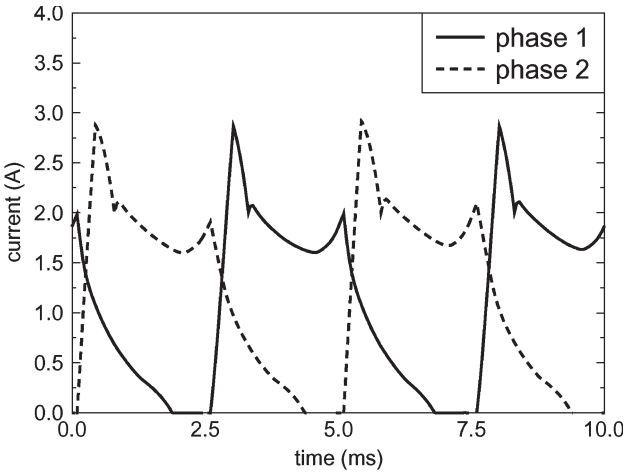

Fig. 5. Simulated currents for the optimized rotor.

efficiency, the input power was measured at the dc link that feeds the converter, and the output power was calculated by torque multiplied by the rotational speed. Thus, the calculated efficiencies are related to the whole set, i.e., the drive circuit plus the motor.

B. Simulation Results

The coupled field-circuit simulation is performed for both rotor types at 6000 r/min. The resulting currents in both phases are shown in Figs. 5 and 6 for the optimized rotor and the reference rotor, respectively. It can be seen that, although the control strategy is identical in both cases, the resulting current is significantly different for both rotor types. Comparing Figs. 4 and 5, sufficient agreement between simulated and measured currents can be observed.

From the electromagnetic field distribution, the generated torque is calculated applying the Maxwell stress tensor. From Fig. 7, it can be seen that the optimized rotor yields significantly less torque ripple in operation at 6000 r/min, which has been confirmed by measurement [1].

In addition to the torque calculations, the surface-force density acting at the stator surface is calculated. Its spectra are shown in Figs. 8 and 9 for circumferential mode $r = 0$ and 2,

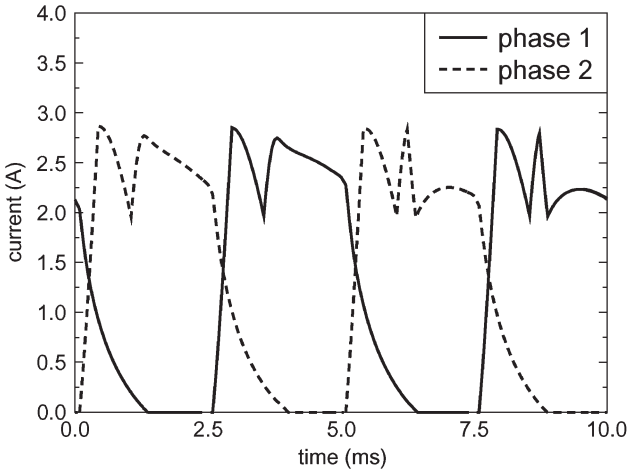

Fig. 6. Simulated currents for the reference rotor.

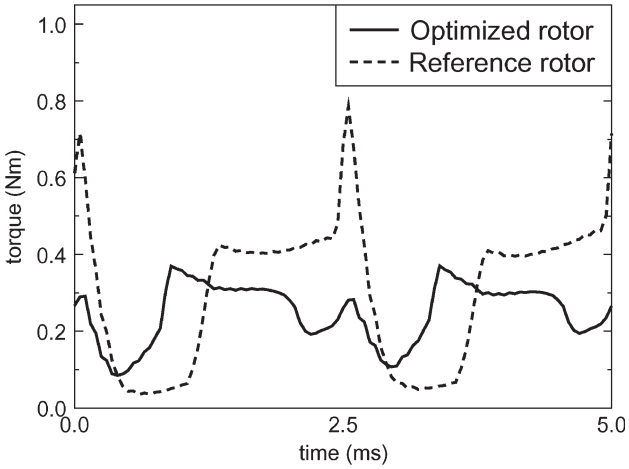

Fig. 7. Simulated torque for the reference and optimized rotors.

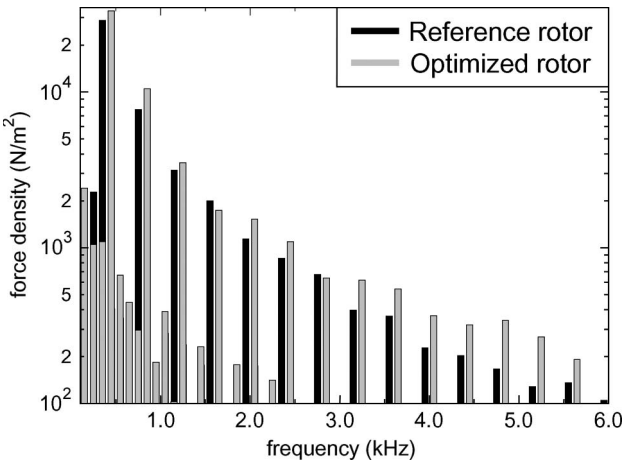

Fig. 8. Simulated force density with mode $r = 0$.

respectively. It can be observed that the superior rotor shape in terms of force excitation clearly depends on the individual frequency. For example, concerning the most important mode $r = 2$, in the frequency range up to 4 kHz, the optimized rotor shows better or approximately equal performance in terms of force excitation, where in the range between 4 and 6 kHz, the

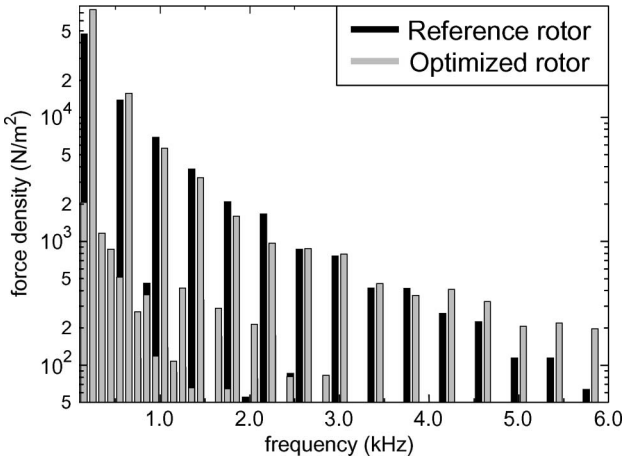

Fig. 9. Simulated force density with mode $r = 2$.

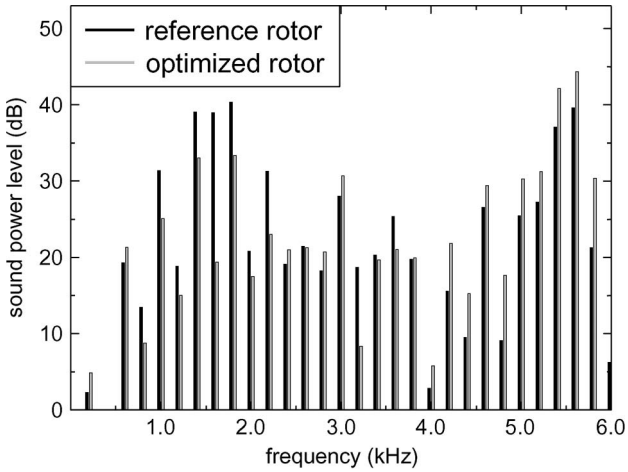

Fig. 10. Simulated sound power level.

force excitation of the optimized rotor is higher. Since the force excitation, driven by the current, has a rectangular waveform, the higher time harmonics are decaying with frequency. Since no clear statement about the influence of the rotor geometry on the acoustic behavior can be made from excitation alone, a structure-dynamic simulation and an acoustic simulation as a subsequent step seem to be reasonable.

As a first step, a numerical modal analysis is performed. Within the frequency range of interest, in this specific application (0–6 kHz), 22 eigenvalues are found. They can be classified into three categories: The first one (up to about 2 kHz) is movements of the stator and housing as a rigid body with respect to the two ground plates, which are defined to have zero deformation as a clamping condition. The movement is carried out by deforming the weld seams. The second group is located between 2 and 2.6 kHz. Here, mostly, the four mounting rods between the front and back plates of the SRM are resonating. Finally, above 2.6 kHz, the front and back plates, as well as the cylindrical body, have resonances.

The total acoustic power, calculated by means of integrating the product of pressure and velocity, is used for the comparison. This is done in the frequency range up to 6 kHz. The result is shown in Fig. 10. It can be seen that, at frequencies up to about 4 kHz, the reference design radiates more acoustic power, where above 4 kHz, the optimized design is disadvantageous in terms of acoustic radiation. To evaluate the total acoustic behavior of both designs, the total acoustic power level is calculated. Since the reference rotor gives 46.7 dB and the optimized rotor gives 47.4 dB, it can be concluded that, in overall, both designs nearly have equal acoustic performance.

As this study is comparing a rotor type that has been optimized for torque ripple with its reference counterpart, a final comparison is given in Table I. It clearly highlights that the optimization is effective, since the side effects, such as decrease of mean torque and increase of total acoustic power, are acceptable.

TABLE I
COMPARISON OF SRM WITH REFERENCE AND OPTIMIZED ROTORS

Value	Reference rotor	Optimized Rotor
Max. phase current (A)	2.85	2.87
Mean phase current (A)	1.31	1.14
Max. torque (Nm)	0.823	0.385
Mean torque (Nm)	0.284	0.267
Torque ripple (Nm)	0.788	0.303
Total sound power level (dB)	46.7	47.4

IV. SUMMARY, CONCLUSION, AND FUTURE WORK

This paper has presented an energy-based field–circuit coupling based on a temporary lumped-parameter model of the magnetic part in combination with a multiphysics simulation of the acoustic radiation of electrical machines.

The harmonic force excitation is calculated by means of a stress tensor computation and transformed to a mechanical mesh by mapping techniques. The structural problem is solved in the frequency domain using FE modal analysis and superposition. The radiation characteristic is obtained from boundary element acoustic simulations.

The proposed method is applied to a special SRM with asymmetric pole geometry to improve start-up torque. The pole shape has been optimized for low torque ripple in a previous work, and the proposed approach is used to analyze the impact of the optimization on the overall acoustic behavior.

Simulation results show sufficient agreement with measured currents. It is shown that the acoustic characteristic of the SRM with optimized rotor is only superior in the lower frequency domain. For frequency larger than approximately 4 kHz, the initial design radiates lower noise. Overall, it can be said that the optimized design is superior, since the torque ripple was decreased significantly and the decrease of mean torque and the increase of total acoustic power are acceptable.

Since the described procedure is costly in terms of computational time, further development will focus on developing a method to define a transfer function which represents the vibroacoustic in a single complex number per frequency and mode. This then can be used to optimize this special SRM for torque ripple, as well as for acoustic radiation at the same time. In addition, the authors are currently working on smart current profiling to minimize the vibration, as, e.g., shown for induction machines in [26].

REFERENCES

[1] S. Nabeta, I. Chabu, L. Lebensztajn, D. Correa, W. da Silva, and K. Hameyer, "Mitigation of the torque ripple of a switched reluctance motor through a multiobjective optimization," *IEEE Trans. Magn.*, vol. 44, no. 6, pp. 1018–1021, Jun. 2008.

[2] N. Sadowski, Y. Lefevre, C. Neves, and R. Carlson, "Finite elements coupled to electrical circuit equations in the simulation of switched reluctance drives: Attention to mechanical behaviour," *IEEE Trans. Magn.*, vol. 32, no. 3, pp. 1086–1089, May 1996.

[3] M. Hecquet and P. Brochet, "Modeling of a claw-pole alternator using permeance network coupled with electric circuits," *IEEE Trans. Magn.*, vol. 31, no. 3, pp. 2131–2134, May 1995.

[4] H. Bai, S. Pekarek, J. Techenor, W. Eversman, D. Buening, G. Holbrook, M. Hull, R. Krefta, and S. Shields, "Analytical derivation of a coupled-circuit model of a claw-pole alternator with concentrated stator winding," *IEEE Power Eng. Rev.*, vol. 21, no. 12, p. 66, Dec. 2001.

[5] A. Canova, M. Ottella, and D. Rodger, "A coupled field–circuit approach to 3D FEM analysis of electromechanical devices," in *Proc. 9th Int. Conf. Elect. Mach. Drives (Conf. Pub. 468)*, 1999, pp. 71–75.

[6] P. Zhou, D. Lin, W. Fu, B. Ionescu, and Z. Cendes, "A general cosimulation approach for coupled field–circuit problems," *IEEE Trans. Magn.*, vol. 42, no. 4, pp. 1051–1054, Apr. 2006.

[7] S. Kanerva, S. Seman, and A. Arkkio, "Inductance model for coupling finite element analysis with circuit simulation," *IEEE Trans. Magn.*, vol. 41, no. 5, pp. 1620–1623, May 2005.

[8] H. Jordan, *Geräuscharme Elektromotoren*, H. Franz, Ed. Essen, Germany: W. Girardet, Nov. 1950.

[9] J. Gieras, C. Wang, and J. C. Lai, *Noise of Polyphase Electric Motors*. Boca Raton, FL: CRC Press, 2006.

[10] J. Le Besnerais, A. Fasquelle, M. Hecquet, J. Pelle, V. Lanfranchi, S. Harmand, P. Brochet, and A. Randria, "Multiphysics modeling: Electro-vibro-acoustics and heat transfer of PWM-fed induction machines," *IEEE Trans. Ind. Electron.*, vol. 57, no. 4, pp. 1279–1287, Apr. 2010.

[11] M. Furlan, A. Cernigoj, and M. Boltezar, "A coupled electromagnetic-mechanical-acoustic model of a DC electric motor," *COMPEL, Int. J. Comput. Math. Elect. Electron. Eng.*, vol. 22, no. 4, pp. 1155–1165, 2003.

[12] C. Schlensok, B. Schmülling, M. van der Giet, and K. Hameyer, "Electromagnetically excited audible noise evaluation and optimization of electrical machines by numerical simulation," *COMPEL, Int. J. Comput. Math. Elect. Electron. Eng.*, vol. 26, no. 3, pp. 727–742, 2007.

[13] K. Vijayakumar, R. Karthikeyan, S. Paramasivam, R. Arumugam, and K. Srinivas, "Switched reluctance motor modeling, design, simulation, and analysis: A comprehensive review," *IEEE Trans. Magn.*, vol. 44, no. 12, pp. 4605–4617, Dec. 2008.

[14] I. Chabu, S. Nabeta, and J. Cardoso, "Design aspects of 4:2 pole-2 phase switched reluctance motors," in *Proc. IEMD Conf.*, May 1999, pp. 63–65.

[15] T. Miller, "Optimal design of switched reluctance motors," *IEEE Trans. Ind. Electron.*, vol. 49, no. 1, pp. 15–27, Feb. 2002.

[16] B. Mirzaeian, M. Moallem, V. Tahani, and C. Lucas, "Multiobjective optimization method based on a genetic algorithm for switched reluctance motor design," *IEEE Trans. Magn.*, vol. 38, no. 3, pp. 1524–1527, May 2002.

[17] E. Lange, F. Henrotte, and K. Hameyer, "A circuit coupling method based on a temporary linearization of the energy balance of the finite element model," *IEEE Trans. Magn.*, vol. 44, no. 6, pp. 838–841, Jun. 2008.

[18] N. Demerdash and T. Nehl, "Electric machinery parameters and torques by current and energy perturbations from field computations. I. Theory and formulation," *IEEE Trans. Energy Convers.*, vol. 14, no. 4, pp. 1507–1513, Dec. 1999.

[19] F. Henrotte and K. Hameyer, "The structure of electromagnetic energy flows in continuous media," *IEEE Trans. Magn.*, vol. 42, no. 4, pp. 903–906, Apr. 2006.

[20] F. Henrotte and K. Hameyer, "A theory for electromagnetic force formulas in continuous media," *IEEE Trans. Magn.*, vol. 43, no. 4, pp. 1445–1448, Apr. 2007.

[21] J. Melcher, *Continuum Electromechanics*. Cambridge, MA: MIT Press, 1981.

[22] S. J. Yang, *Low-Noise Electrical Motors*, S. J. Yang, Ed. Oxford, U.K.: Clarendon, 1981.

[23] O. Zienkiewicz and R. Taylor, *The Finite Element Method*, 4th ed. London, U.K.: McGraw-Hill, 1991.

[24] S. Long, Z. Zhu, and D. Howe, "Vibration behaviour of stators of switched reluctance motors," *Proc. Inst. Elect. Eng.—Electr. Power Appl.*, vol. 148, no. 3, pp. 257–264, May 2001.

[25] R. D. Ciskowski and C. A. Brebbia, *Boundary Element Methods in Acoustics*. Amsterdam, The Netherlands: Elsevier, 1991.

[26] A. Ruiz-Gonzalez, M. Meco-Gutierrez, F. Perez-Hidalgo, F. Vargas-Merino, and J. Heredia-Larrubia, "Reducing acoustic noise radiated by inverter-fed induction motors controlled by a new PWM strategy," *IEEE Trans. Ind. Electron.*, vol. 57, no. 1, pp. 228–236, Jan. 2010.

M. van der Giet was born in Krefeld, Germany, in 1977. He received the Dipl.-Ing. (M.Sc.) degree in electrical engineering from the Faculty of Electrical Engineering and Information Technology, RWTH Aachen University, Aachen, Germany, in 2004, where he is currently working toward the Ph.D. degree in the area of noise and vibration of electrical machines.

Since 2004, he has been a Researcher at the Institute of Electrical Machines, RWTH Aachen University, where he became the Chief Engineer in 2008.

E. Lange was born in 1978. He received the Dipl.-Ing. (M.Sc.) degree in electrical engineering from RWTH Aachen University, Aachen, Germany, in 2006.

Since 2006, he has been a Research Associate at the Institute of Electrical Machines, RWTH Aachen University. His research interests are numerical field computation and multiphysics modeling with a focus on electrical machines.

D. A. P. Corrêa received the B.Sc. degree from Maua Institute of Technology, São Caetano do Sul, Brazil, in 2003, and the M.Sc. degree in electrical engineering from the Escola Politécnica da Universidade de São Paulo (EPUSP), São Paulo, Brazil, in 2009.

Since 2001, he has been working at Centro Tecnológico da Marinha on research and development projects. His research interests are power electronics and control and simulation.

I. E. Chabu received the B.Sc., M.Sc., and D.Sc. degrees in electrical engineering from the Escola Politécnica da Universidade de São Paulo (EPUSP), São Paulo, Brazil, in 1978, 1990, and 1997, respectively.

Since 1990, he has been a Lecturer in the Department of Electrical Engineering, EPUSP, where he is involved in several research projects. His academic activity concerns graduate and postgraduate courses. His main areas of interest are electrical machines, linear motors for industrial applications, and electrical traction. He specializes in the design and construction of electrical machinery and electromechanical devices.

S. I. Nabeta received the B.Sc. and M.Sc. degrees in electrical engineering from the Escola Politécnica da Universidade de São Paulo (EPUSP), São Paulo, Brazil, in 1983 and 1990, respectively, and the Ph.D. degree in electrical engineering from the Institut National Polytechnique de Grenoble, Grenoble, France, in 1994.

He is currently an Associate Professor at EPUSP. His main research interests are analytical and numerical modeling of electrical machines, numerical techniques, and electric traction.

K. Hameyer (M'96–SM'99) received the M.Sc. degree in electrical engineering from the University of Hannover, Hannover, Germany, the Ph.D. degree from the University of Technology Berlin, Berlin, Germany, and the Dr.Habil. degree from the Faculty of Electrical Engineering, Technical University of Poznan, Poznan, Poland, in 2004.

Until February 2004, he was a Full Professor at the Katholieke Universiteit Leuven, Leuven, Belgium. He is currently the Director of the Institute of Electrical Machines, RWTH Aachen University, Aachen, Germany. His research interests are numerical field computation, design and control of electrical machines, and numerical optimization strategies.

Dr. Hameyer is a Fellow of the Institution of Engineering and Technology (IET), U.K. He is an elected member of the Board of the International Compumag Society and a founding member of the executive team of the IET Professional Electromagnetics Network. He was awarded the title of Dr.h.c. from the Faculty of Electrical Engineering, Technical University of Cluj Napoca, Cluj Napoca, Romania.